Contents lists available at ScienceDirect

Heliyon

Research article

Rational sonochemical engineering of Ag_2CrO_4/g-C_3N_4 heterojunction for eradicating RhB dye under full broad spectrum

Ali Alsalme [a], Mohamed M. Hassan [b], Mohamed A. Eltawil [b], A.E. Amin [b], Ayman Soltan [c], M.F. Abdel Messih [b], M.A. Ahmed [b],*

[a] Department of Chemistry, College of Science, King Saud University, P.O.2455, Riyadh, 11451, Saudi Arabia
[b] Chemistry Department, Faculty of Science, Ain Shams University, Egypt
[c] Department of Chemistry, University of York, York, YO10 5DD, UK

A R T I C L E I N F O

A B S T R A C T

In this novel research, S-scheme Ag_2CrO_4/g-C_3N_4 heterojunctions were generated by sono-chemical hybridization of different compositions of Ag_2CrO_4 nanoparticles [E_{VB} = +2.21 eV] and g-C_3N_4 sheets [E_{CB} = −1.3 eV] for destructing RhB dye under artificial solar radiation. The as-synthesized nanocomposites were subjected to X-ray diffraction [XRD], diffuse reflectance spectrum [DRS], X-ray photoelectron spectroscopy [XPS], N_2-adsorption-desorption isotherm, photoluminescence [PL] and high resolution transmission electron microscope [HRTEM] analysis to explore the interfacial interactions between g-C_3N_4 sheets and Ag_2CrO_4 nanoparticles. Spherical Ag_2CrO_4 nanoparticles deposited homogeneously on the wrinkles points of g-C_3N_4 sheets at nearly equidistant from each other facilitating the uniform absorption of solar radia-tions. The absorbability of solar radiations was enhanced by introducing 20 wt % Ag_2CrO_4 on g-C_3N_4 sheets. The surface area of g-C_3N_4 sheets was reduced from 37.5 to 16.4 m^2/g and PL signal intensity diminished by 80 % implying the successful interfacial interaction between Ag_2CrO_4 nanoparticles and g-C_3N_4 sheets. The photocatalytic performance of heterojunctions containing 20 % Ag_2CrO_4 and 80 % g-C_3N_4 destructed 96 % of RhB dye compared with 60 and 33 % removal on the surface of pristine g-C_3N_4 sheets and Ag_2CrO_4, respectively. Benzoquinone and ammonium oxalate are strongly scavenged the dye decomposition revealing the strong influence of valence band holes of Ag_2CrO_4 and superoxide radicals in destructing RhB dye under solar radiations. S-scheme charge transportation mechanism was suggested rather than type II heterojunction on the light of scavenger trapping experiments results and PL spectrum of terephthalic acid. Overall, this research work illustrated the manipulation of novel S-scheme heterojunction with efficient redox power for destructing various organic pollutants persisted in water resources.

1. Introduction

Wastewater emerged from various industry is rich with toxic pollutants that threat human health and aquatic life with serious problems. Biological treatment, ion-exchange, adsorption and reverse osmosis processes are high cost, energy consumer and still embedded secondary generation of pollutants that require additional treatment [1–5]. The expelling of toxic organic pollutants from

---

* Corresponding author.
  E-mail address: abdelhay71@hotmail.com (M.A. Ahmed).

wastewater under solar radiations is required for environmental purposes [6–10]. Photocatalysis green technology required a low cost semiconductor and available light source [11–15]. Single photocatalysts displayed poor efficiency for producing reactive oxygen species that need for fragmentation of organic pollutants due to the fast and uncontrolled rate of Coulombic interactions between positive holes and negative electrons. An additional dilemma is concerned with weak absorbability of the single photocatalyst to solar radiations. By considering the above aspects, a successful heterojunction is needed to generate huge amount of electron-hole pairs with better separation and transportation efficiency. The g-C$_3$N$_4$ sheets exhibit non-toxicity, low cost, simple route of preparation and adjustable band gap energy [16–20]. Dilemma, the fast electron-hole Coulombic attraction force and the weak charge transportation reduced the photocatalytic efficiency. Hybridizing graphitic carbon nitride with effective semiconductor of aligned band gap structure is attractive route for generating successful heterojunctions with extra-ordinary redox power and superior charge separation and transportation. The g-C$_3$N$_4$ sheets with 2.8 eV band gap energy and conduction band potential E$_{CB}$ = −1.3 eV is promising reductive photocatalyst for destructing dye molecules and producing superoxide radicals. Concurrently, Silver chromate with 1.9 eV band gap energy and valence band potential E$_{VB}$ = +2.2 eV is effective oxidative photocatalyst due to the unique crystalline and electronic properties and availability of producing large concentration of electron-hole pairs on the solid surface [21–25]. Dilemma, the sparingly solubility in aqueous medium and the photocorrosion of silver chromate under light illumination reduced the photocatalytic efficiency and stability. Coupling silver chromate with g-C$_3$N$_4$ is best issue for limiting the shortcoming of single g-C$_3$N$_4$ and Ag$_2$CrO$_4$ molecules through fabrication of S-scheme heterojunction with proper electron-hole separation and transportation [26–32]. Yu et al. prepared Ag$_2$CrO$_4$/Ag/g-C$_3$N$_4$ for photodegradation of methyl orange dye and the experimental results have pointed out that Ag$_2$CrO$_4$ enhanced the separation efficiency of the charge carrier separation and enhanced the photocatalytic activity of the solid specimen in dye degradation. They recorded that the positive holes and superoxide radicals are the efficient species involved in the degradation process rather than hydroxyl radicals [26]. Ren et al. synthesized hollow mesoporous g-C$_3$N$_4$/Ag$_2$CrO$_4$ by simple precipitation method for mitigation of rhodamine B and tetracycline. The hollow mesoporous configuration trapped strongly the incident photons for elevating the absorption of visible light radiations [27]. Rajalakshmi et al. synthesized g-C$_3$N$_4$/Ag$_2$CrO$_4$ by hydrothermal method for photo-catalytic degradation of 2-nitrophenol under visible irradiations. The exceptional photocatalytic reactivity was ascribed to the pro-duction of large amount of reactive species through construction of S-scheme Ag$_2$CrO$_4$/g-C$_3$N$_4$ heterojunction [28]. A successful photocatalytic hydrogen production was carried out on the surface of Ag$_2$CrO$_4$/g-C$_3$N$_4$ heterojunctions. This promising heterojunction profited the photocatalytic reaction with electrons of strong reducing power for hydrogen gas production [29]. Akhundi et al. prepared AgI and Ag$_2$CrO$_4$ on g-C$_3$N$_4$/Fe$_3$O$_4$ by co-deposition route for mitigation of rhodamine B dye under solar radiations. The nano-composite exhibited high photocatalytic efficiency in degrading rhodamine B dye compared with the pristine semiconductor which
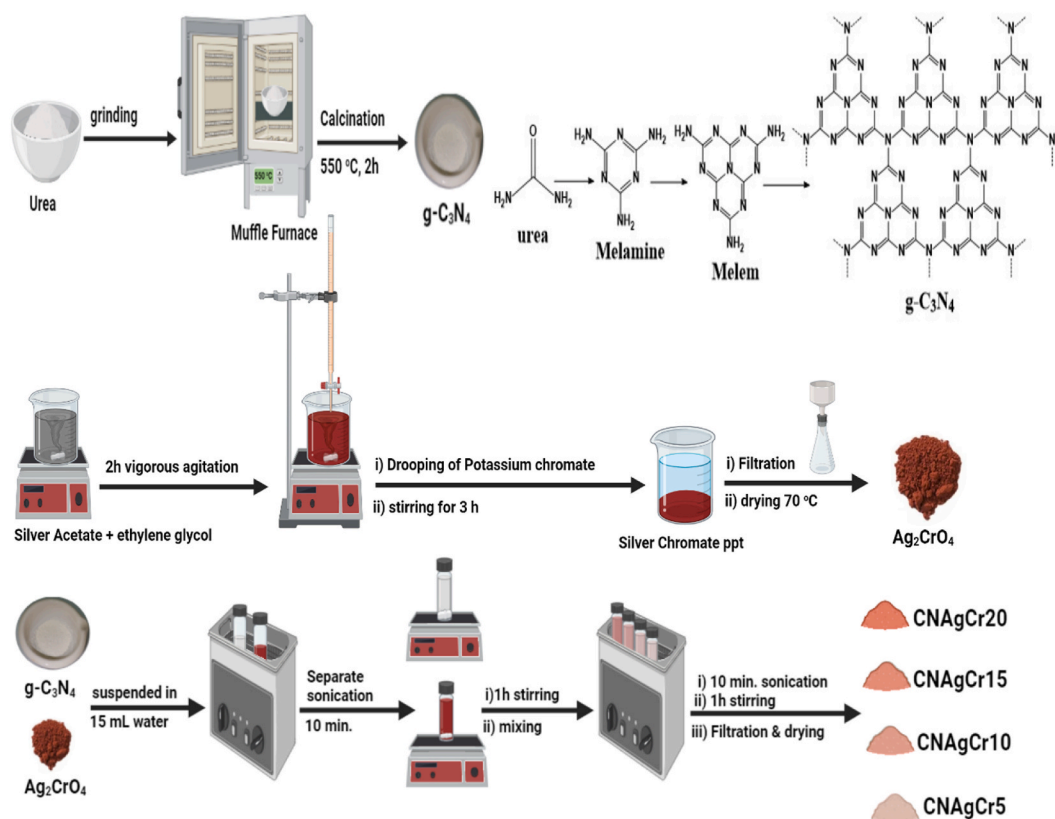

Fig. 1. Scheme for preparation route of (a) g-C$_3$N$_4$, (b) Ag$_2$CrO$_4$ and (c) CNAgCr20.

ascribed to the better charge transportation and separation [30]. Aziz Habibi-Yangjeh et al. synthesized g-C_3N_4/Fe_3O_4/Ag_2CrO_4 containing 20 wt% of Ag_2CrO_4 by reflux method for eliminating RhB from aqueous solution [31]. Shang et al. recorded that 95 % of RhB dye was mineralized over Ag_2CrO_4/g-C_3N_4 containing 30 wt% Ag_2CrO_4 nanocomposite synthesized by microemulsion assisted precipitation method [32]. The extraordinary photocatalytic reactivity was ascribed to the tendency of Ag_2CrO_4 nanoparticles in enhancing the charge carrier separation, reduced the grain size and inhibited the corrosion of Ag_2CrO_4. No previous research was carried out on sonochemical synthesis and investigation of Ag_2CrO_4/g-C_3N_4 nanocomposites for various photocatalytic applications. In our novel research, we make an attempts for sonochemical synthesis of S-scheme Ag_2CrO_4/g-C_3N_4 heterojunctions containing different compositions of Ag_2CrO_4 and g-C_3N_4 for photocatalytic destruction of rhodamine B dye under artificial solar radiations. The physicochemical properties were investigated by XRD, HRTEM, BET, PL and DRS analysis. The photocatalytic performance of Ag_2CrO_4/g-C_3N_4 heterojunctions for photocatalytic expelling of rhodamine B dye were tested and compared with the pristine nanoparticles under the same operating conditions. The photocatalytic mechanism and the charge transportation were suggested and illustrated adopting S-scheme route. The experimental results of this research can borrow the environmental photocatalysis with novel and efficient heterojunctions with extra-ordinary redox power for destructing various organic pollutants.

2. Materials and methods

2.1. Material

Rhodamine B, Microcrystalline urea, Silver acetate, Terephthalic acid, Ammonium oxalate, Potassium chromate, Isopropanol and Benzoquinone with purity 99 % are captured from Riedel Company.

2.2. Preparation of the photocatalyst

2.2.1. Thermal synthesis of pristine g-C_3N_4 sheets
120 g of microcrystalline urea was directed to thermal reactor with large diameter to homogenize the effect of the thermal operating conditions to all solid matrix [Fig. 1]. The thermal reactor was positioned in the furnace and the temperature was elevated from ambient temperature to 525 °C by rate 2 °C/min. The furnace was kept at 525 °C for 4 h to stabilize the phase transformation. It is interesting to notice a huge amount of vapors emerged from the furnace starting from 400 to 460 °C due to condensation of urea and expelling of ammonia gas. After the thermal treatment stage, the furnace was closed and the system was cooled to the ambient temperature under room operating conditions overnight. On the next day, the furnace was opened and the porcelain mortar containing the spongy g-C_3N_4 powder with remarkable voids result from vapor evolution was taken off. The solid sheets were grinding and preserved in falcon tube.

2.2.2. Preparation of Ag_2CrO_4 nanoparticles
3 g of silver acetate (99.9 %) dissolved in freshly prepared distilled water was sonicated for 15 min in glass reactor. In another cleaned glass reactor, 1.5 g of potassium chromate dissolved in distilled water was subjected to ultrasonic bath for 15-min. The above solutions were mixed together in ultrasonic bath of 200 W power and sonicated for 40-min. The dark red sol observed manifested the production of Ag_2CrO_4 nanoparticles. The solution was filtered, washed with distilled water and acetone and dried at 85 °C overnight. The dried solid specimen was collected and grinding in porcelain mortar and preserved in falcon tube.

2.2.3. Preparation of Ag_2CrO_4/g-C_3N_4
S-scheme Ag_2CrO_4/g-C_3N_4 heterojunctions with rational compositions of Ag_2CrO_4 nanoparticles and g-C_3N_4 sheets were synthesized sonochemically [Fig. 1]. Two separated glass reactor containing definite proportions of g-C_3N_4 and Ag_2CrO_4 nanoparticles dispersed in distilled water were sonicated for 20 min. Afterwhile, the constituent of the two reactors were mixed in the ultrasonic bath. The mixture solution was sonicated for 40-min at 30 °C to absorb sufficient ultrasonic energy which produce various bubbles and cavity in the solution medium. Then, the sonicated mixture separated by filtration system, washed with distilled water. Finally, the solid heterojunction was dried at 90 °C for 12 h and grinding into porcelain mortar and sieved. The solid specimens were denoted as g-C_3N_4, Ag_2CrO_4, CNAgCr5, CNAgCr10, CNAgCr15, CNAgCr20 and CNAgCr25 for pristine g-C_3N_4, Ag_2CrO_4 and the heterojunctions containing 5, 10, 15, 20 and 25 wt% Ag_2CrO_4, respectively.

2.3. Material characterization

The crystalline compositions of the as synthesized solid specimens were explored by P'Analytical X'PERT MPD diffractometer. The textural parameters including pore structure, surface area and BET-C-constant were determined by adsorption isotherms of N_2 gas on the solid surface at 77 K. HRTEM JEOL 6340 determined the mode of dispersion of Ag_2CrO_4 nanoparticles on g-C_3N_4 surface and the particle size of the photocatalyst. JASCO spectrometer (V-570) constructed an absorption spectrum curve to determine the band gap structure. Thermo Fischer spectrometer recorded PL spectrum of solid sample by taking 380 nm as excitation wavelength for comparing the separation efficiency of the heterojunctions with the pristine nanoparticles. The photocatalytic fragmentation of RhB dye under solar simulator was investigated on the pristine nanoparticles and heterojunction constitute [5–25] wt % of Ag_2CrO_4. In each photocatalytic degradation experiment, 0.05 g of the photocatalyst was dispersed in 100 ml of 2×10^{-5} M RhB dye solution with constant agitation with rate 250 rpm/min under dark conditions for 1 h to achieve adsorption-desorption equilibrium. Afterwhile, a

solar simulator with 300 W power was switched on the above mixture for 2 h and at constant interval times, 4-ml of the pollutant solution was separated with syringe, centrifuged, and the color intensity of the remainder solution was recorded by Jusco UV–Visible spectrophotometer.

3. Results and discussions

3.1. Physicochemical characterization

XRD analysis investigated the crystalline features of g-C_3N_4, Ag_2CrO_4 and Ag_2CrO_4/g-C_3N_4 heterojunction [Fig. 2]. Two remarkable diffraction peaks with average width are labelled at 2Θ = 13.2 and 27.2° to identify (100) and (002) planes of g-C_3N_4 orthorhombic structure ((JCPDS no: 87–1526). The diffraction pattern of Ag_2CrO_4 recorded various crystalline peaks at 2θ = 17.7, 21.8, 25.4, 31.3, 31.6, 32.3, 33.8, 39.1, 44.3, 45.4, 52.2, 55.9, 57.1, 61.9 and 62.9 ascribed to Ag_2CrO_4 orthorhombic crystalline phase [JCPDS file no. of 26–0952]. XRD pattern of CNAgCr20 showed characteristic diffraction peaks assigned to the co-existence of both g-C_3N_4 and Ag_2CrO_4 orthorhombic phases. The crystalline peaks of orthorhombic g-C_3N_4 and Ag_2CrO_4 were slightly shifted to lower values reflecting the successful construction of Ag_2CrO_4/g-C_3N_4 heterojunction [Fig. 2]. The crystallite size calculated adopting Scherrer equation was 25.2 and 97.5 for pristine g-C_3N_4 and Ag_2CrO_4, respectively. On the other hand, the crystallite size of g-C_3N_4 and Ag_2CrO_4 in the heterojunction CNAgCr20 was 12.3 and 57.4 nm for g-C_3N_4 and Ag_2CrO_4, respectively. The depression in the particle size resulted from the successful deposition of Ag_2CrO_4 on g-C_3N_4 sheets surface under sonochemical conditions. In fact, sonochemical route generates large amount of bubbles and air cavities that restrict the particles agglomeration and reduced the particle dimensions. N_2-adsorption-desorption isotherms of g-C_3N_4 and CNAgCr20 were illustrated in Fig. 3a and b, respectively for investigating the textural structure of the solid specimens and determine the surface area and pore dimensions. In agreement with BDDT classification, type II isotherm is appropriate for recording the adsorption mechanism of N_2 molecules on the photocatalyst surface. This isotherm is ascribed to non-porous surface configuration for solid surface that facilitating the approach of dye molecules to solid surface without any restrictions imposed by pore dimensions. The specific surface area of the pristine g-C_3N_4 sheets and CNAgCr20 heterojunction was 37.4 and 16.5 m^2/g, respectively as determined by mathematical exploration of BET equation in its accepted P/Po data range that is usually collected between 0.005 and 0.3 P/Po values. The total pore volume was 0.41 and 0.185 cm^3/g for g-C_3N_4 and CNAgCr20, respectively. These textural experimental results implied that incorporation of 20 wt% Ag_2CrO_4 reduced the surface area and the total pore volume to half its values revealing the coverage of nearly half number of g-C_3N_4 active sites with Ag_2CrO_4 molecules. It is interesting to notice that BET-C constant increased from 50 to 479 with introduction of 20 wt % Ag_2CrO_4. In fact, the BET-C constant is direct measurement of the strength of solid-gas interaction implying that introducing Ag_2CrO_4 on g-C_3N_4 surface increased the surface polarity. Although, the adsorption-desorption isotherms are completely revisable, the corresponding Va-t plot for g-C_3N_4 and CNAgCr20 recorded in Fig. 3d and e, respectively showed an upward deviation implying the existence of some pores falls in the range of wide micropores or narrow mesopores. HRTEM illustrated the production of g-C_3N_4 sheets with fragile and sponge features [Fig. 4a]. Small spheres of Ag_2CrO_4 nanoparticles were dispersed homogeneously on various active centers of g-C_3N_4 sheets [Fig. 4b]. SAED analysis was recorded in Fig. 4c and d for g-C_3N_4 sheets and CNAgCr20, respectively. SAED image recorded two diffraction ring ascribed to (100) and (002) crystalline planes of orthorhombic g-C_3N_4 sheets [Fig. 4c]. However, SAED image of CNAgCr20 showed various diffraction rings referred to both crystalline phases of orthorhombic g-C_3N_4 and Ag_2CrO_4 implying the successful construction of Ag_2CrO_4/g-C_3N_4 heterojunction. [Fig. 4d]. The elemental composition and the oxidation state of CNAgCr20 heterojunction were
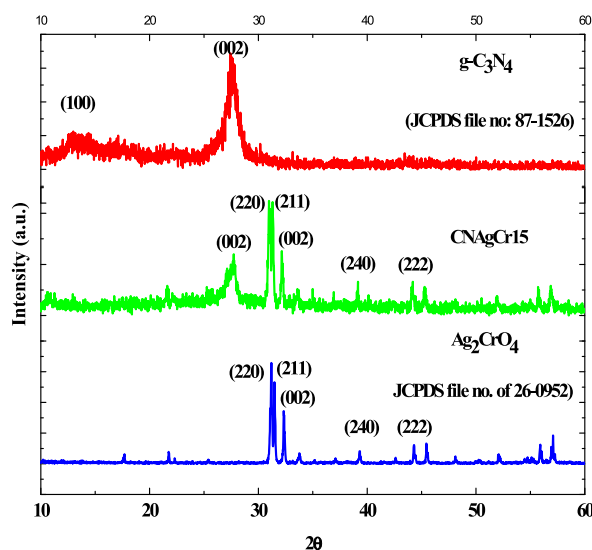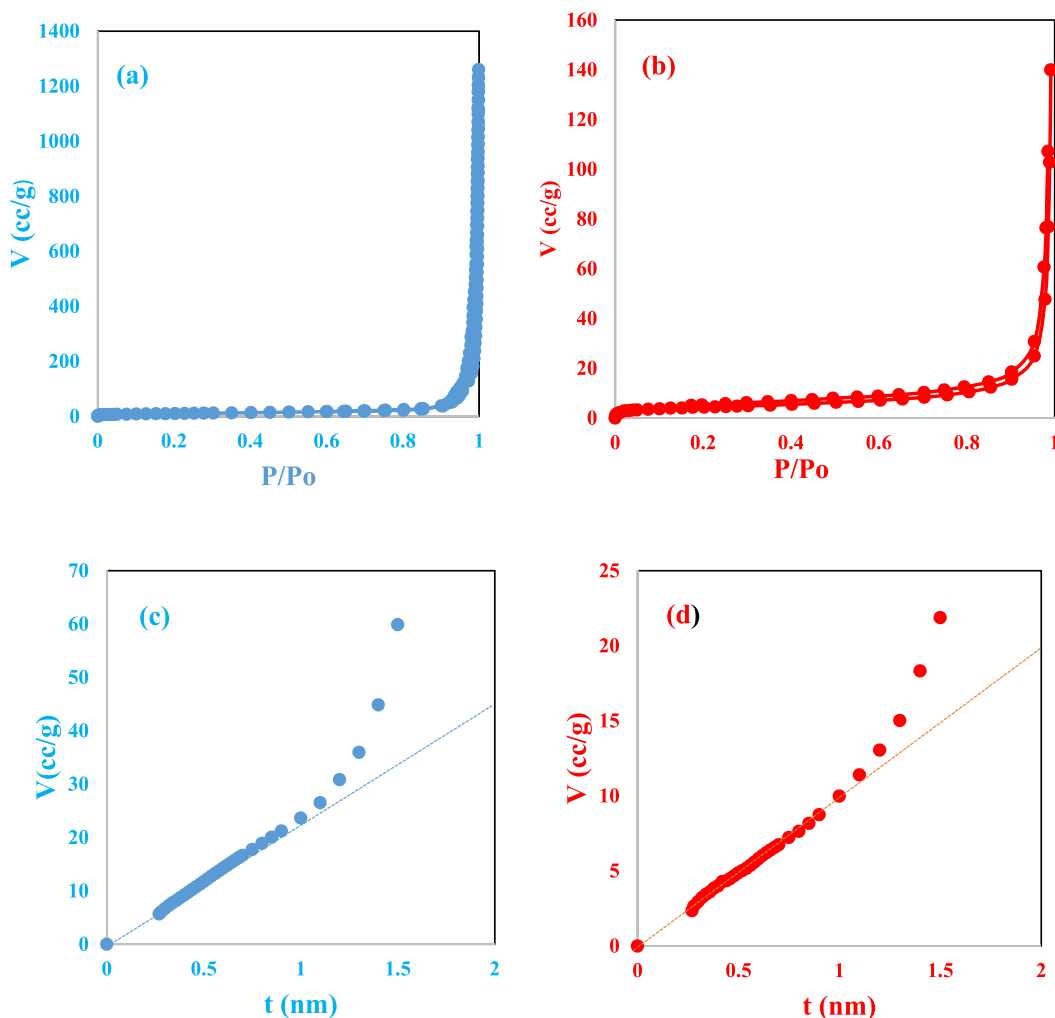

Fig. 2. XRD pattern of g-C_3N_4, Ag_2CrO_4 and CNAgCr20 heterojunction.

Fig. 3. N_2-adsorption-desorption isotherm of (a) g-C_3N_4 and (b) CNAgCr20, (c) V_l-t plot of g-C_3N_4 and (d) V_l-t plot of CNAgCr20.

investigated by high resolution X-ray photoelectron spectrum [XPS] measurements [Fig. 5]. The spectrum show several peaks assigned to C, N, Ag, Cr and O elements revealing the high purity of the as synthesized sample [Fig. 5a]. The C 1s spectrum are resolved into three deconvoluted peaks at 284.6 eV, 285.7 eV, 288.1 eV and 288.9 eV which ascribed to C–C bonds, sp² hybrid C atoms in the N–C––N groups of tri-s-triazine rings and C atoms in the C–NH groups, respectively [Fig. 5b]. The N 1s spectrum are resolved into three deconvoluted peaks at 398.9 eV, 399.7 eV and 400.4 eV which ascribed to the N atoms in C–N––C groups, the tertiary N atoms in N-$(C)_3$ groups and the N atoms in the N–H groups in tri-s-triazine ring, respectively [Fig. 5c]. There are three O 1s deconvoluted peaks at 530.4 eV, 531.7 eV and 534.3 eV, respectively. The deconvoluted peak at 530.4 eV corresponds to the lattice oxygen atoms and the other two O 1s deconvoluted peaks resulted from adsorbed hydroxyl groups and water molecules, respectively [Fig. 5d]. Fig. 5e showed two deconvoluted peaks at 367.8 eV and 373.8 eV, corresponding to the electron spin states of Ag $3d_{5/2}$ and Ag $3d_{3/2}$ respectively The spectrum of Cr^{6+} 2p are resolved into two deconvoluted peaks at 577.3 eV and 586.8 eV correspond to the electron spin states of Cr $2p_{3/2}$ and Cr $2p_{1/2}$ respectively [Fig. 5f]. The deconvoluted peak at 574.9 eV is ascribed to Ag (3p). DRS spectrum was constructed in Fig. 6 to shed light on the absorbability of pristine g-C_3N_4 sheets, Ag_2CrO_4 nanoparticles and CNAgCr20 heterojunction. The absorbability of g-C_3N_4 sheets was directed toward initial region of visible region spectrum [Fig. 6a] with band gap energy of 2.8 eV as reported extensively in the previous recent researches [26–28,33]. On the other hand, Ag_2CrO_4 recorded an absorption edge in the deep visible region with band gap energy of 1.91 eV implied the beneficial absorption of large portion of solar spectrum by Ag_2CrO_4 nanoparticles. A remarkable shift in the absorbability of g-C_3N_4 was recorded by hybridizing g-C_3N_4 sheets with Ag_2CrO_4 nanoparticles which taken as benefits for absorption of large fraction of solar radiation. DRS spectrum of CNAgCr20 illustrated two absorption edges at 2.6 and 1.9 eV manifested the successful construction of Ag_2CrO_4/g-C_3N_4 heterojunction which ascribed to the absorbability of g-C_3N_4 sheets and Ag_2CrO_4 in deep visible region [Fig. 6b]. Compared with g-C_3N_4, the photon harvesting activity of Ag_2CrO_4/g-C_3N_4 nanocomposite materials in a range of 300–700 nm gradually increases with introducing Ag_2CrO_4 nanoparticles revealing that the enhanced photocatalytic performance was attributed to the strong electron coupling between g-C_3N_4 sheets and Ag_2CrO_4
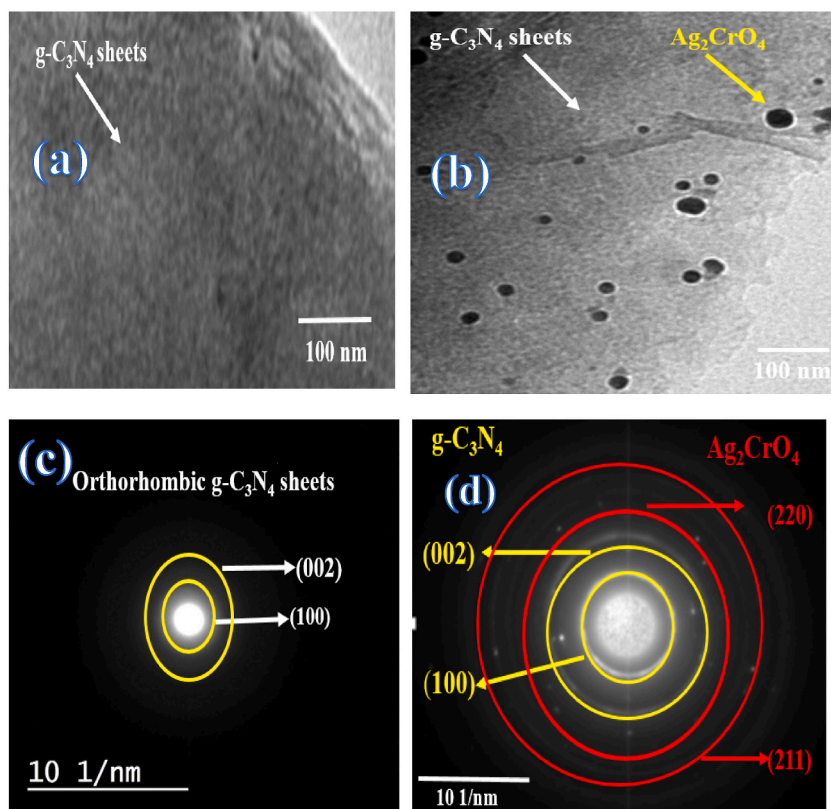
Fig. 4. High resolution transmission electron microscope [HRTEM] of (a) g-C$_3$N$_4$ and (b) CNAgCr20, Selected area electron diffraction [SAED] of (c) g-C$_3$N$_4$ and (d) CNAgCr20.

nanoparticles. Yu et al. recorded a red shift in the absorption end with incorporation of various compositions of Ag$_2$CrO$_4$ on g-C$_3$N$_4$ surface in agreement with our experimental results [26]. The valence and conduction band potential was calculated by Kubelka-Munk equation based on the electronegativity of g-C$_3$N$_4$ and Ag$_2$CrO$_4$. The valence and conduction band of Ag$_2$CrO$_4$ calculated are 2.21 and +0.3 eV. On the other hand, the valence and conduction band of g-C$_3$N$_4$ are 1.5 and −1.3 eV. PL spectrum of the as-synthesized solid specimens determined the efficiency of electron-hole pairs separation and transportation [Fig. 7]. The stronger emission PL signal intensity resulted in higher recombination rate of electron-hole pairs that limited the number of free holes and electrons. Pristine g-C$_3$N$_4$ sheets displayed strong PL emission signal centered at 433 nm resulted from high rate of charge carriers recombination [Fig. 7]. Surprisingly, incorporation of various proportions Ag$_2$CrO$_4$ was impulsively decremented the PL signal intensity revealing the successful enhancement of electron-hole separation that increased the life time of Ag$_2$CrO$_4$ positive holes and g-C$_3$N$_4$ negative electrons for redox processes. The intensity of PL signal was reduced by 60, 68, 82 and 88 % with incorporation of 5, 10, 15 and 20 wt% Ag$_2$CrO$_4$, respectively. These experimental results manifested that Ag$_2$CrO$_4$ nanoparticles depressed the electron-hole recombination and increases in the life time of the photocatalyst in destructing organic molecules.

3.2. Photocatalytic degradation of rhodamine B dye

Rhodamine B dye is an attractive dye employed in capacious industrial applications owing to its auspicious florescent red color. This cationic dye possesses strong stable chemical structure resulted from the conjugated aromatic system that resist the mineralization under chemical and biological treatment. Various scenario were postulated to get rid of this toxic dye through adsorption, biological treatment, coagulation and ion exchange processes. However, these methods failed to break down the stable chemical dye molecules in accompanied to transportation of the primary dye structure to secondary generation of pollutants. Expelling of rhodamine B under solar radiations on low cost semiconductor surface is attractive clean technology for environmental applications. The absorption spectrum for photocatalytic degradation of RhB dye over pristine g-C$_3$N$_4$, AgCrO$_4$ and AgCrO$_4$/g-C$_3$N$_4$ heterojunctions was recorded in Fig. 8. The absorbance intensity of RhB dye decreased gradually with increasing illumination time implied the cleavage of rhodamine B molecules under the influence of solar radiations and reactive oxygen species into a series of organic RhB derivatives that decomposed finally into CO$_2$ and H$_2$O. Several signals were positioned at wave length of 554, 537, 525, and 490 nm which ascribed to N, N-tri-ethylated rhodamine, N,N –di-ethylated rhodamine and N-ethylated rhodamine, respectively. On comparing the depression in RhB dye concentration under dark conditions on the surface of Ag$_2$CrO$_4$/g-C$_3$N$_4$ containing various proportions of Ag$_2$CrO$_4$, one can realized that the amount of dye expelled through adsorption process not exceed 10 %. This experimental result manifested that the attraction
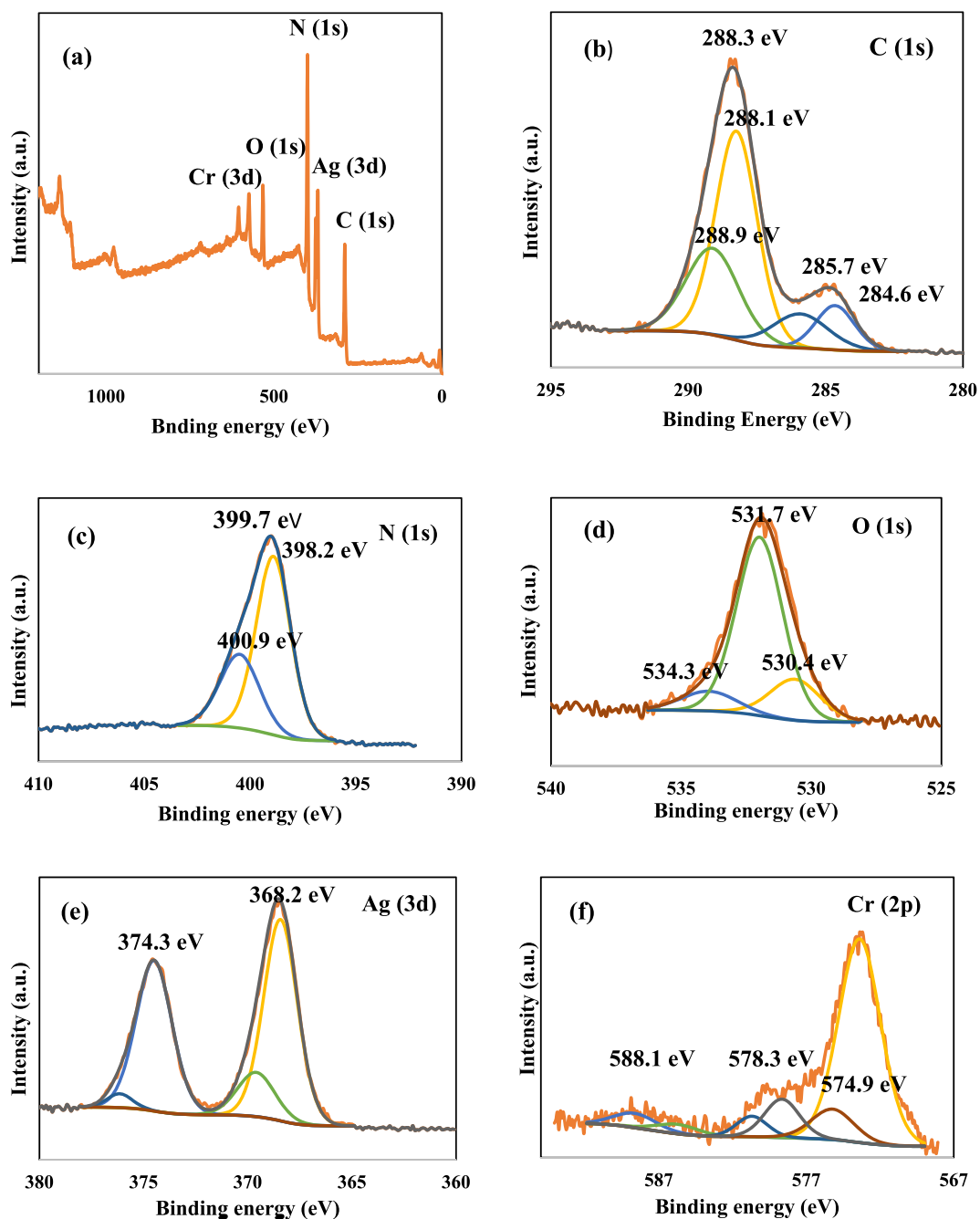
Fig. 5. (a) XPS survey spectra of CNAgCr20. High resolution XPS spectra of C 1s (b), N 1s (c), O 4f (d), Ag 3d (e) and Cr 3d (f).

forces between dye molecules and surface of all solid specimens is weak and exhibit little influence on total dye degradation. On switching the solar simulator of 300 W power, a rapid depression in the absorbance intensity was detected due to the fragmentation of RhB dye into smaller molecules simultaneously. 60 %, 33 %, 64 %, 68 %, 80 %, 94 % and 53 % of RhB dye was decomposed on the surface of g-C_3N_4, Ag_2CrO_4, CNAgCr5, CNAgCr10 CNAgCr15, CNAgCr20 and CNAgCr25, respectively after 2 h of light illumination [Fig. 9a]. By following the photocatalytic rate of RhB dye decomposition over pristine g-C_3N_4 sheets and Ag_2CrO_4/g-C_3N_4 hetero-junctions, the experimental data revealed that the fragmentation of RhB obeyed pseudo-first order reaction [Fig. 9b and c]. The pseudo-first order rate constant for decomposition of RhB dye calculated from the graphical plot is 0.022, 0.003, 0.0114, 0.023, 0.037, 0.039 and 0.019 min^{-1} over g-C_3N_4, Ag_2CrO_4, CNAgCr5, CNAgCr10 CNAgCr15, CNAgCr20 and CNAgCr25, respectively. The rate of RhB dye decomposition on Ag_2CrO_4 surface was nearly half than that over pristine g-C_3N_4 sheets which ascribed to the narrow band gap energy of Ag_2CrO_4 (Eg = 1.9 eV) compared with that of g-C_3N_4 (Eg = 2.8 eV) which lead to fast electron-hole Columbic attraction
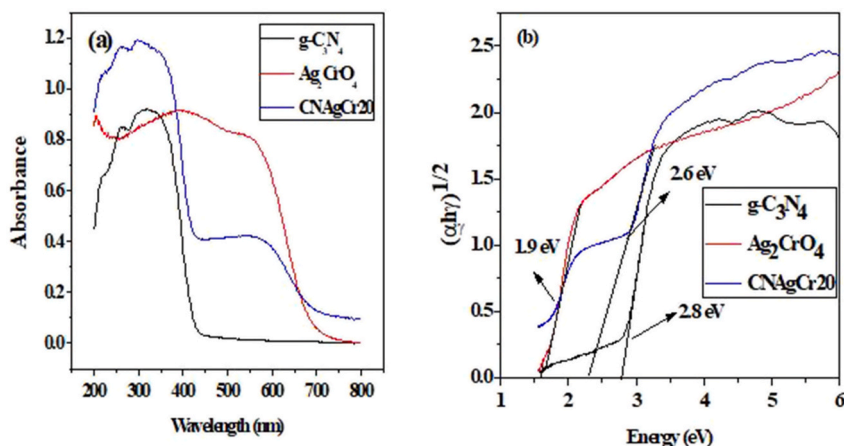
Fig. 6. (a) Diffuse reflectance spectrum [DRS] of g-C_3N_4, Ag_2CrO_4 and CNAgCr20, (b) Tauc plots of g-C_3N_4, Ag_2CrO_4 and CNAgCr20.
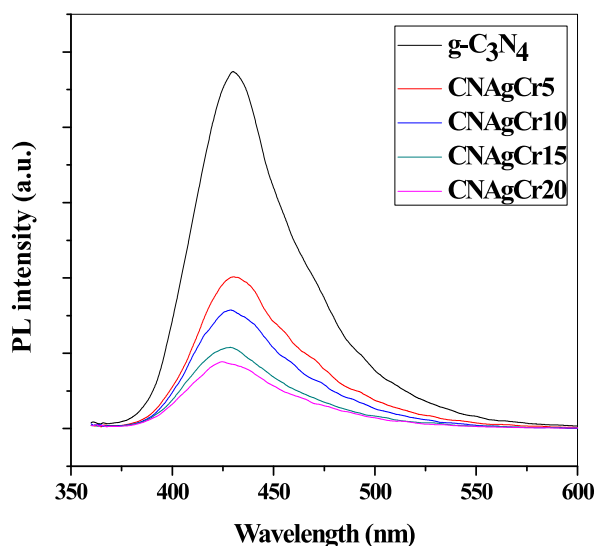
**Fig. 7.** Photoluminescence [PL] analysis of g-C_3N_4, CNAgCr5, CNAgCr10, CNAgCr15, CNAgCr20.

force. This strong recombination rate between electron-hole pairs on Ag_2CrO_4 surface reduced the production of charge carriers and reactive oxygen species which depressed the mineralization rate. Introducing 5, 10, 15 and 20 wt % of Ag_2CrO_4 nanoparticles elevated the rate of RhB dye decomposition which ascribed to the positive role of Ag_2CrO_4 in enhancing the absorbability of g-C_3N_4 to deep visible region and improving the efficiency of electron-hole separation. These experimental evidence extracted from PL analysis indicated that deposition of 20 wt% Ag_2CrO_4 on g-C_3N_4 surface depressed 80 % of the rate of charge carrier recombination. Further, increase loading of 25 wt % Ag_2CrO_4 depressed the degradation rate to half its value compared with the optimum sample CNAgCr20 which ascribed to the production of passive layers of Ag_2CrO_4 that inhibited the interaction between the light photons and the heterojunction surface. These fruitless layers retarded the immigration of electron-hole pairs to the interface region between heterojunction-dye solutions to generate the reactive oxygen molecules. The quantitative results for RhB mitigation over pristine g-C_3N_4 sheets and heterojunctions containing [0–25] wt% Ag_2CrO_4 implied that deposition of 20 wt% Ag_2CrO_4 is the optimal composition for attaining the maximum degradation rate which is in agreement with work of Aziz Habibi-Yangjeh [31] that recorded that 20 wt% Ag_2CrO_4 optimized the rate of RhB degradation over g-C_3N_4/Fe_3O_4/Ag_2CrO_4 nanocomposites prepared by reflux route. To determine the role of reactive species that responsible for fragmentation of RhB dye, three different scrubbers with the same concentration of 1×10^{-3} M were mixed with CNAgCr20 photocatalyst-dye solution mixture under the same operating condition of the photocatalytic process [Fig. 10a–d]. The experimental results indicated that the amount of dye degraded reduced from 94 to 23 % and 47 % in presence of benzoquinone and ammonium oxalate scrubbers, respectively. These scrubber experimental analysis implied that positive holes and superoxide radicals are primary reactive species in expelling RhB dye under solar radiations. The rate of RhB degradation depressed from 0.0248 to 0.0013 and 0.01 min^{-1} in presence of benzoquinone and ammonium oxalate, respectively revealing that the influence of superoxide radicals is more precocious than positive holes. On the other hand, mixing the mixture of
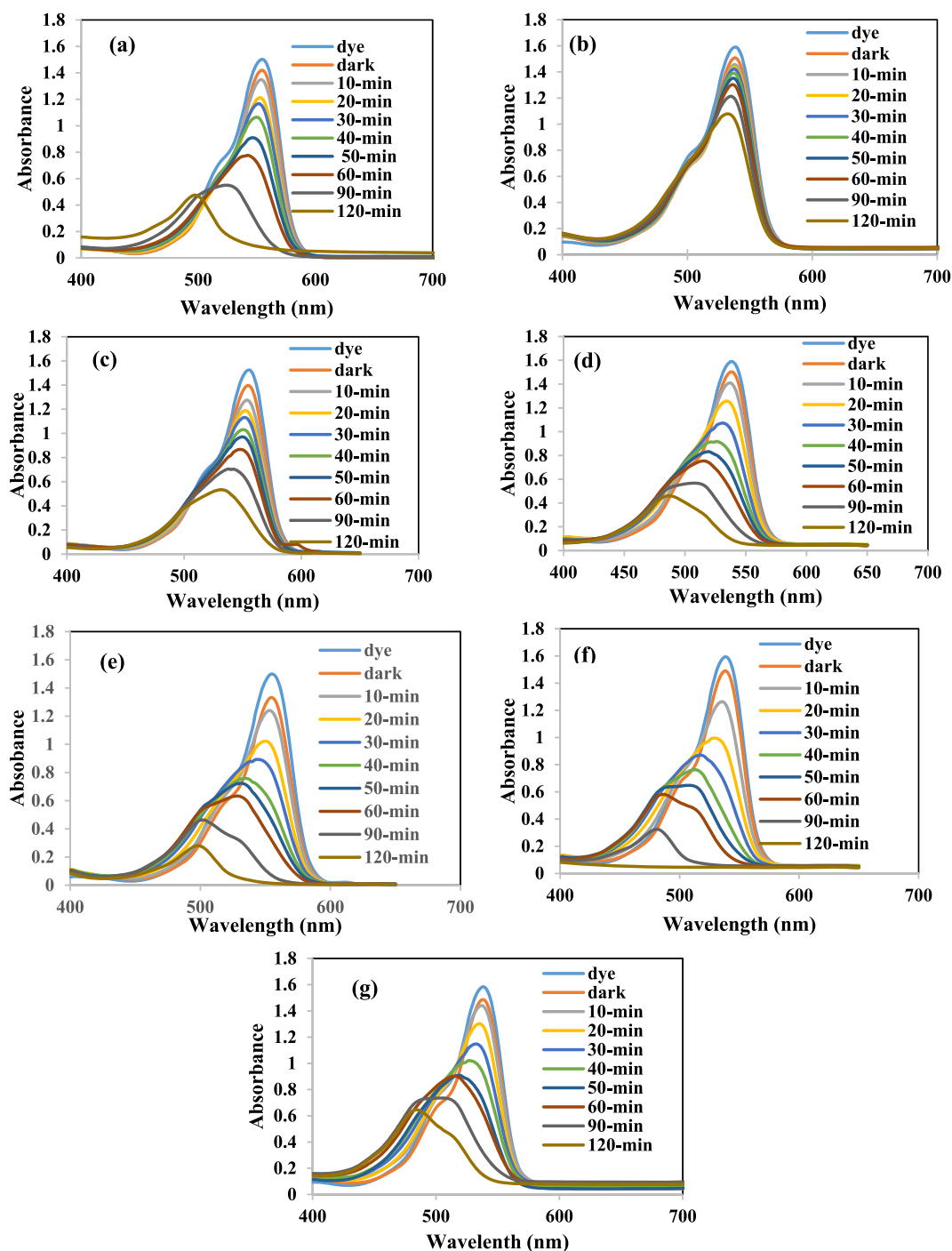
Fig. 8. The absorption spectrum of photocatalytic degradation of rhodamine B dye over the surface of (a) g-C$_3$N$_4$, (b) Ag$_2$CrO$_4$, (c) CNAgCr5, (d) CNAgCr10, (e) CNAgCr15, (f) CNAgCr20 and (g) CNAgCr25.

solid-dye solution with isopropanol depressed the degradation rate from 0.0248 to 0.0243 min^{-1} implied that hydroxyl radicals show weak contribution to the degradation process. These results agreed with work of Aziz Habibi-Yangjeh et al. [31] that recorded that positive holes and superoxide radicals of prime important role in expelling RhB under visible light on surface of AgI/Ag$_2$-CrO$_4$/g-C$_3$N$_4$/Fe$_3$O$_4$ ternary nanocomposites [30]. Moreover, Ren et al. [27] experimental work manifested the positive role of superoxide and positive role in accelerating the photodegradation of tetracycline and rhodamine B dye on the surface of hollow Ag$_2$CrO$_4$/g-C$_3$N$_4$ mesoporous nanocomposite synthesized by silica hard template. PL analysis of terephthalic acid was carried out to investigate the production of hydroxyl groups under light illumination [Fig. 11]. PL spectrum displayed an emission peak centered at
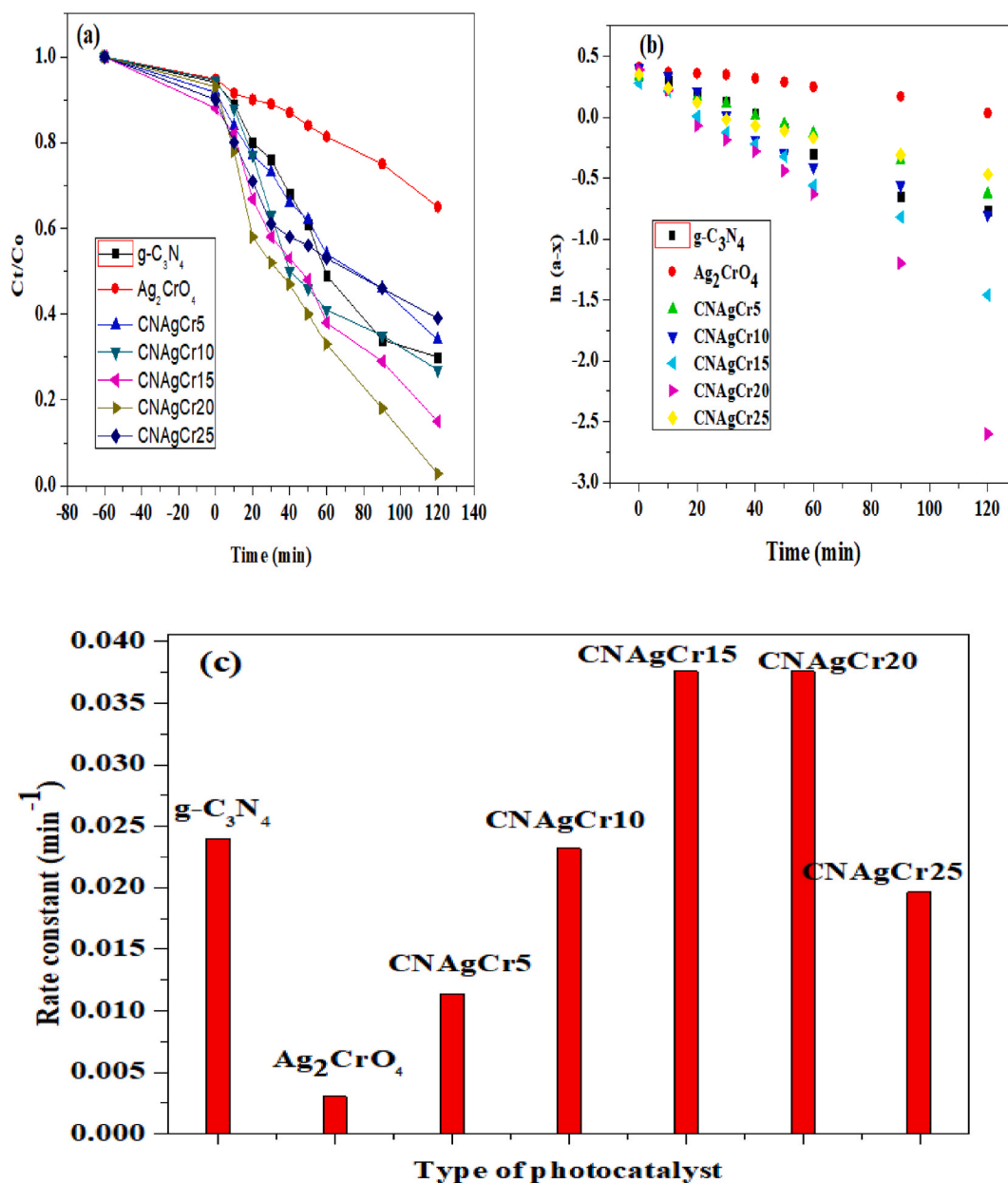
Fig. 9. (a) The variation of the removal of RhB dye over the surface of the pristine and the as-synthesized heterojunctions with time of irradiations, (b) The first order kinetics plot of photocatalytic degradation of RhB over the surface of the as-synthesized samples, (c) The variation of pseudo-first order rate constant for photodegradation of RhB dye with the composition of Ag_2CrO_4 in the heterojunctions.

423 nm revealed the production of hydroxyl radicals under solar radiations. This experimental result revealed the production of hydroxyl radicals by water oxidation [$E_{OH-/OH.} = +1.88$ eV] under the influence of positive hole of valence band of Ag_2CrO_4 [$E_{VB} = +2.21$ eV]. However, the positive hole of g-C_3N_4 [$E_{VB} = +1.5$ eV] cannot produce hydroxyl radicals. The experimental quantitative analysis of kinetics calculation for rate of expelling RhB under solar radiations in presence and absence of scrubber species can be explained in the light of valence and conduction band of the two semiconductors. The high reduction potential of g-C_3N_4 ($E_{CB} = -1.3$ eV) can generate superoxide radicals ($E_{O2/O2-.} = -0.34$ eV) by reduction of adsorbed oxygen with conduction band electrons. The valence band of Ag_2CrO_4 is 2.21 eV can produce hydroxyl radicals by hydroxyl ion oxidation [$E_{OH/OH.} = +1.88$ eV]. This result manifested that superoxide and hydroxyl radicals are the most reactive species involved in the photocatalytic degradation of RhB dye. Total organic carbon [TOC] was measured to confirm the complete degradation of RhB dye into eco-friendly species rather than decolorization process. TOC content reduced from 55.2 mg/l to 3.7 mg/l confirmed the mineralization of RhB rather than decolorization process.
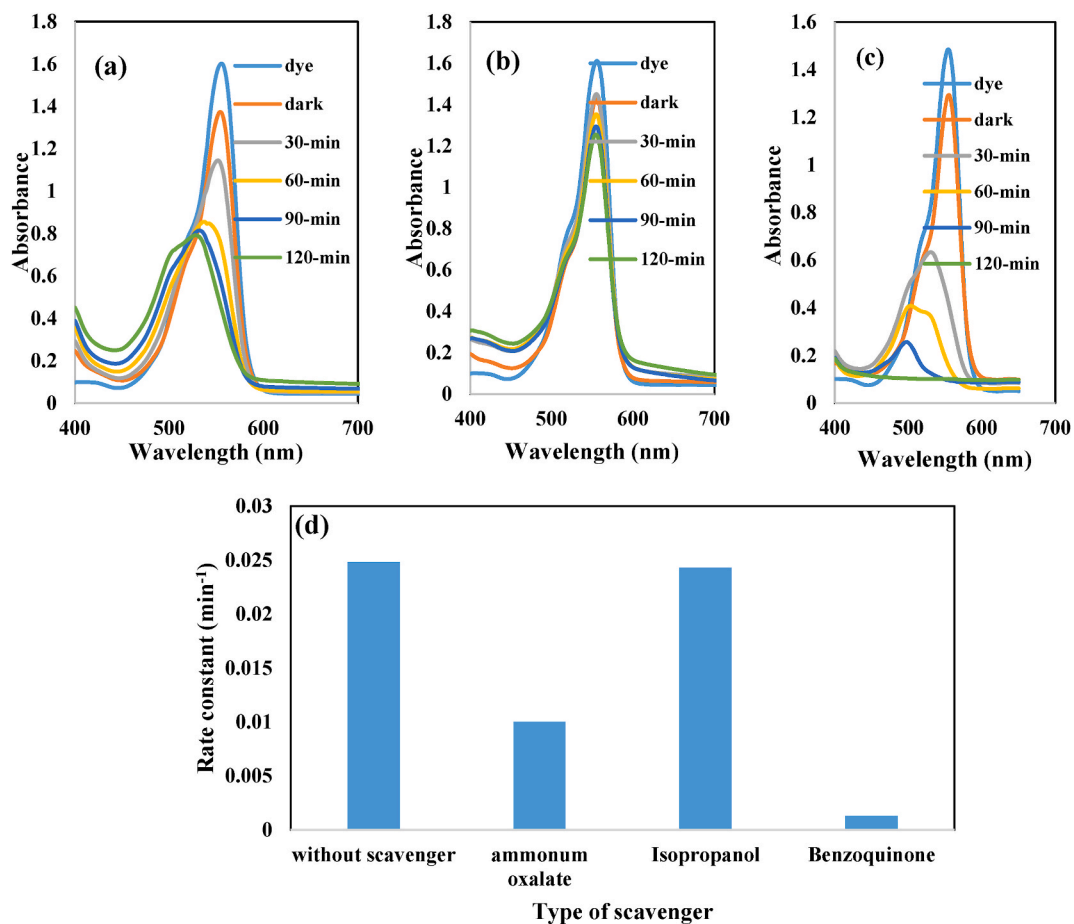
Fig. 10. The photocatalytic degradation of RhB dye over the surface of CNAgCr20 heterojunction in presence of (a) ammonium oxalate, (b) benzoquinone and (c) isopropanol as trapping molecules (d) The variation of rate constant for photodegradation of RhB dye with different types of scavengers.
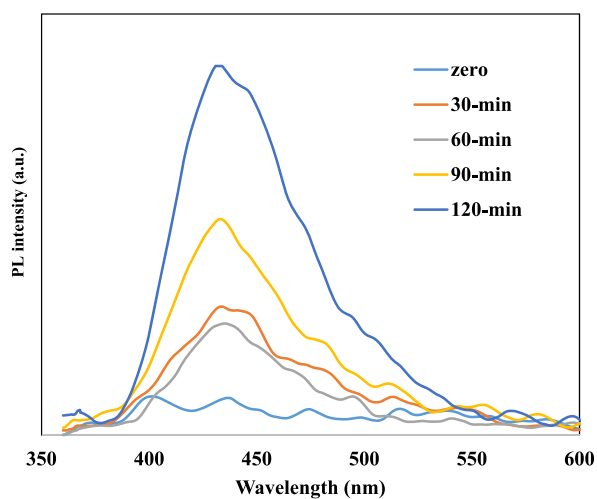
Fig. 11. PL spectrum of terephthalic acid over CNAgCr20 under light illumination.

The photocatalytic process is usually initiated by absorption of sufficient photon energy that must equal to or higher than the difference in energy between valence and conduction band of the two semiconductors [Fig. 12]. The charge transportation mechanism can be proceeded through different routes as straddling, type II heterojunction, Z-scheme and S-scheme mechanism. The proper predication of the actual mechanism is determined from the band gap energy, the valence and conduction band potential of each semiconductor. The valence and conduction band potential was calculated by Kubelka-Munk equation based on the electronegativity of g-C_3N_4 and Ag_2CrO_4. The valence and conduction band of Ag_2CrO_4 calculated are 2.21 and +0.3 eV. On the other hand, the valence and conduction band of g-C_3N_4 are 1.5 and −1.3 eV. The evidence for the proper calculation of valence and conduction band of both semiconductors and the mechanism of charge transportation are verified from scavenger trapping experiments [Fig. 10] and PL analysis of terephthalic acid under light illumination [Fig. 11]. PL spectrum illustrated the increasing in the emission peak intensity recorded at 423 nm with increasing the time of light illumination. This result revealed the production of hydroxyl radicals [$E_{OH-/OH.=+}$1.88 eV] from oxidation of hydroxyl anions by positive holes of valence band of Ag_2CrO_4 [E_{VB} = +2.21 eV]. However, the positive holes of the valence band of g-C_3N_4 [E_{VB} = +1.5 eV] cannot produce hydroxyl radicals [$E_{OH-/OH.}$ = +1.88 eV]. On the other hand, the scavenger trapping experiments revealed that the rate of RhB destruction is strongly depressed by adding benzoquinone as scavenger for superoxide radicals [$E_{O2-/O2.}$ = -0.34 eV]. This result implied that superoxide radicals was generated from reduction of adsorbed oxygen by electrons conduction band of g-C_3N_4 [E_{CB} = −1.3 eV]. However, the electrons conduction band of Ag_2CrO_4 [E_{CB} = +0.3 eV] cannot produce superoxide radicals [$E_{O2-/O2.}$ = -0.34 eV]. The results extracted from scavenger experiments and PL analysis of terephthalic acid under light illumination manifested the predication of valence and conduction band of Ag_2CrO_4 and g-C_3N_4 after contact and proved that the mechanism of charge transportation is proceeded through S-scheme route rather than type II heterojunction. As in type II heterojunction, the electrons are transferred from the more negative conduction band of g-C_3N_4 [E_{CB} = −1.3 eV] to conduction band of Ag_2CrO_4 [E_{CB} = +0.3 eV]. By this way, electrons in conduction band of Ag_2CrO_4 cannot produce superoxide radicals [$E_{O2-/O2.}$ = -0.34 eV]. On the other hands, the positive holes are transferred from the more positive valence band of Ag_2CrO_4 [E_{VB} = +2.21 eV] to the valence band of g-C_3N_4 [E_{VB} = +1.5 eV] which failed to produce hydroxyl radicals [$E_{OH-/OH.=+}$1.88 eV]. The production of superoxide and hydroxyl radicals as proved from scavenger experiments and PL of terephthalic acid is solid proof that type II heterojunction failed to explain the proper way of charge transportation. However, adopting S-scheme mechanism, the fruitless electrons and holes of Ag_2CrO_4 [E_{CB} = +0.3 eV] and g-C_3N_4 [E_{VB} = +1.5 eV] with low redox power are recombined and vanished through Coulombic attraction force. However, the electrons and holes in the conduction band of g-C_3N_4 and Ag_2CrO_4 with strong redox power are available to involve in the photocatalytic process to produce huge amount of superoxide and hydroxyl radicals. Adopting S-scheme mechanism [Fig. 12], the heterojunction composed of oxidative photocatalyst of high oxidation potential and reductive photocatalyst with more negative conduction band potential [34–41]. Under light illumination, the electrons are transferred from valence to conduction band leaving positive holes and negative electrons. The electrons in the conduction band of semiconductor of more reductive potential g-C_3N_4 [E_{CB} = −1.3 eV] and higher Fermi level relaxed spontaneously to the conduction band of the other semiconductor Ag_2CrO_4 [E_{CB} = +0.3 eV] of low Fermi level and higher work function. Concurrently, a depletion layer was constructed at the interface region of g-C_3N_4 reductive photocatalyst and an accumulation layer is generated at the interface region of Ag_2CrO_4 oxidative photocatalyst. The g-C_3N_4 sheets are positively charges and Ag_2CrO_4 nanoparticles are negatively charged. The positive holes of g-C_3N_4 attracted the negative electrons of Ag_2CrO_4. These fruitless electron-hole pairs with low redox potential were excluded through strong Coulombic attraction force. Concurrently, the electron-hole pairs of strong redox power in g-C_3N_4 and Ag_2CrO_4 energy levels with E_{VB} = +2.2 eV and E_{CB} = −1.3 eV were ready to borrow in the photocatalytic reaction. This spectacle represent the construction of S-scheme mechanism as target heterojunction with charge carriers with adequate redox potential for employing in capacious photocatalytic process. Table 1 recorded removal of various organic dyes on surface of Ag_2CrO_4 doped with g-C_3N_4 sheets prepared by different routes as precipitation, mechanical grinding, and microemulsion and reflux methods. The experimental results emerged from our research supported that the strong efficiency of our photocatalyst synthesized by low cost sonochemical route in degrading RhB dye under solar radiations. However, the other synthesis routes reported in the previous researches are complicated, expansive and require an addition of third component to attain strong photocatalytic activity.

4. Conclusion

In this novel research, S-scheme sonicated Ag_2CrO_4/g-C_3N_4 heterojunctions were fabricated for efficient photocatalytic destruction of RhB dye under solar radiations. The as-synthesized photocatalysts were fully characterized by DRS, BET, XRD, XPS, HRTEM, PL and SAED analysis. A deep reddish Ag_2CrO_4 nanoparticles enhanced the absorbability of visible light radiations of the heterojunctions compared with pristine g-C_3N_4. 20 wt% Ag_2CrO_4 depressed 80 % of electron-hole Coulombic attraction force and facilitated the charge separation and transportation. The photocatalytic performance of the heterojunction compared with pristine nanoparticles was tested by following the degradation RhB under solar radiations. The experimental results implied that the heterojunction contain 80 % of g-C_3N_4 and 20 wt % Ag_2CrO_4 nanoparticles recorded an optimum expelling of 96 % of RhB dye under solar radiations of 300 W power. The scrubber experimental results implied that superoxide radicals and positive holes exerted the large contribution in fragmentation of RhB dye. S-scheme heterojunction containing Ag_2CrO_4 as oxidative photocatalyst and g-C_3N_4 as reductive species was verified from scavenger trapping experiments.

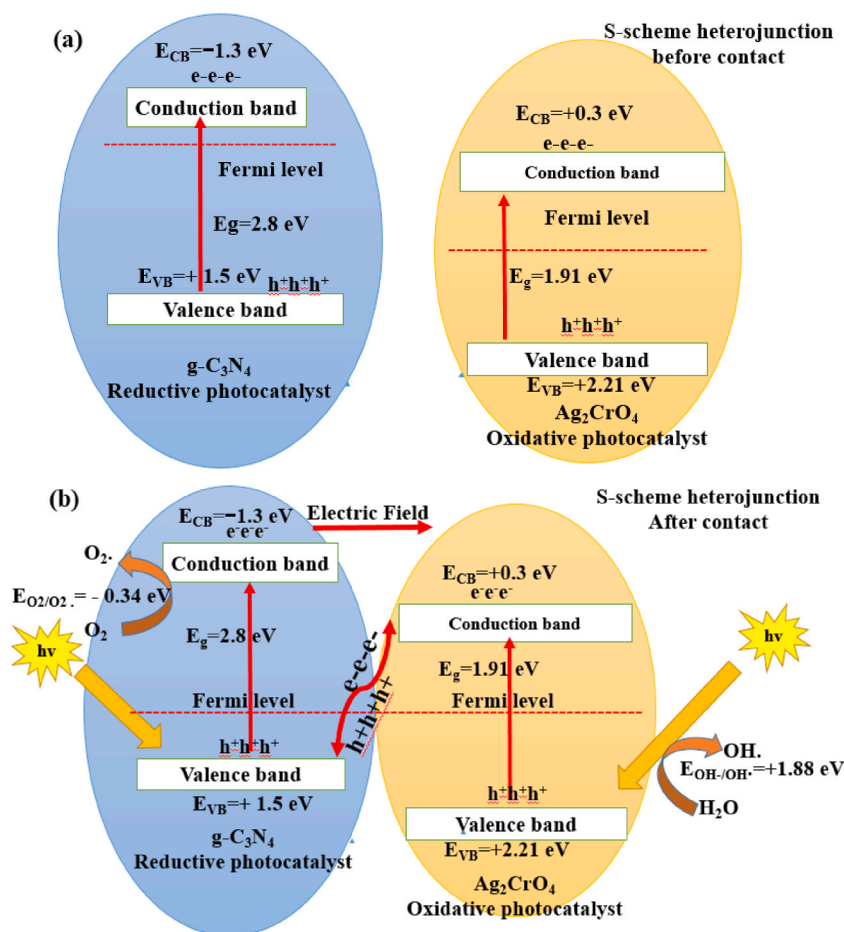## Data availability statements

Data will be made available on request.

Fig. 12. A plausible charge transportation mechanism between g-C$_3$N$_4$ and Ag$_2$CrO$_4$ semiconductors (a) before contact and (b) after contact.

Table 1

Comparative study of photocatalytic degradation of rhodamine B over Ag$_2$CrO$_4$ loaded semiconductors.

Photocatalyst	Mode of preparation	Light source	(%) of dye removal	Reference
Ag$_2$CrO$_4$/g-C$_3$N$_4$	Sonochemical	300 W Solar simulator	95 % of rhodamine B	our research
g-C$_3$N$_4$/Ag/Ag$_2$CrO$_4$	Precipitation	500W Xenon lamp	92 % of Methyl orange	27
g-C$_3$N$_4$/Ag$_2$CrO$_4$	Precipitation	100 W halogen lamp	95 % of rhodamine B	28
Ag$_2$CrO$_4$/g-C$_3$N$_4$	Mechanical grinding	300 W Xenon lamp	94 % of p-nitrophenol	29
AgI/Ag$_2$CrO$_4$/g-C$_3$N$_4$/Fe$_3$O$_4$	Co-deposition	50 W LED lamp	93 % of rhodamine B	31
g-C$_3$N$_4$/Fe$_3$O$_4$/Ag$_2$CrO$_4$	Refluxing	50 W LED lamp	90 % of Rhodamine B	32
Porous g-C$_3$N$_4$/Ag$_2$CrO$_4$	Microemulsion assisted precipitation	300 W Xenon lamp	95 % of Rhodamine B	33

CRediT authorship contribution statement

Ali Alsalme: Investigation, Formal analysis, Funding acquisition. **Mohamed M. Hasan:** Formal analysis, Data curation. **Mohamed A. Eltawil:** Formal analysis, data curation, Investigation. **A.E. Amin:** Investigation, Data curation. **Ayman Soltan:** Methodology, Investigation. **M.F. Abdel Messih:** Formal analysis, Data curation. **M.A. Ahmed:** Writing – review & editing, Visualization, Supervision.

Declaration of competing interest

The authors declare that they have no known competing financial interests or personal relationships that could have appeared to influence the work reported in this paper.

Acknowledgment

We are grateful for the financial supported by Researchers Supporting Project number (RSP2024R78), King Saud University, Riyadh, Saudi Arabia.

References

[1] M.A. Ahmed, Z.M. Abou-Gamra, Mesoporous MgO nanoparticles as a potential sorbent for removal of fast orange and bromophenol dyes, Nanotechnol. Environ. Eng. 1 (10) (2016) 2–11.

[2] M. Adel, M.A. Ahmed, A.A. Mohamed, Effective removal of cationic dyes from aqueous solution using reduced graphene oxide functionalized with manganese ferrite nanoparticles, Compos. Commun. 22 (2020) 100450.

[3] M. Adel, M.A. Ahmed, M. Adel, M.A. Ahmed, A.A. Mohamed, Synthesis and characterization of magnetically separable and recyclable crumbled MgFe2O4/ reduced graphene oxide nanoparticles for removal of methylene blue dye from aqueous solutions, J. Phys. Chem. Solid. 149 (2021) 109760.

[4] Mahmoud Adel, Mohamed A. Ahmed, Ashraf A. Mohamed, A facile and rapid removal of cationic dyes using hierarchically porous reduced graphene oxide decorated with manganese ferrite, Flat Chem. 26 (2021) 100233.

[5] M. Adel, M.A. Ahmed, M.A. Elabiad, A.A. Mohamed, Removal of heavy metals and dyes from wastewater using graphene oxide-based nanomaterials: a critical review, Environ. Nanotechnol. Monit. Manag. 18 (2022) 100719.

[6] M.A. Ahmed, Fahmy Ahmed, M.G. Abo-Zaed, E.M. Hashem, Fabrication of novel AgIO4/SnO2 heterojunction for photocatalytic hydrogen production through direct Z-scheme mechanism, J. Photochem. Photobiol., A 400 (2020) 112660.

[7] Z.M. Abou-Gamra, M.A. Ahmed, M.A. Hamza, Investigation of commercial PbCrO4/TiO2 for photodegradation of rhodamine B in aqueous solution by visible light, Nanotechnol. Environ. Eng. 2 (2017) 12.

[8] M. Abd Elnaby Wafi, M.A. Ahmed, Hesham S. Abdel-Samad, H.A.A. Medien, Exceptional removal of methylene blue and p-aminophenol dye over novel TiO2/ RGO nanocomposites by tandem adsorption-photocatalytic processes, Mater. Sci. for Energy Technol. 5 (2022) 217–231.

[9] M.A. Ahmed, M.F. Abdel-Messih, Eman H. Ismail, Facile synthesis of novel microporous CdSe/SiO2 nanocomposites selective for removal of methylene blue dye by tandem adsorption and photocatalytic process, J. Mater. Sci. Mater. Electron. 30 (2019) 17527–17539.

[10] Alsulmi Ali, N. Mohammed Nagy, Ayman Soltan, M.F. Abdel Messih, M.A. Ahmed, Engineering S-scheme CuO/ZnO heterojunctions sonochemically for eradicating RhB dye from wastewater under solar radiation, RSC Adv. 13 (2023) 13269.

[11] M.A. Ahmed, Nabil Al-Zaqri, Alsalme Ali, A.H. Glal, Mahmood Esa; Rapid photocatalytic degradation of RhB dye and photocatalytic hydrogen production on novel curcumin/SnO2 nanocomposites through direct Z-scheme mechanism, J. Mater. Sci. Mater. Electron. 31 (21) (2020) 19188–19203.

[12] Hashem El-Hussein, Fahmy Ahmed, Abbas Ahmed, Tarek Mohamed, Blal Mahran, M.A. Ahmed, Fabrication of novel AgIO4/TiO2 heterojunction for photocatalytic hydrogen production through direct Z-scheme mechanism, Nanotechnol. Environ. Eng. 5 (2020) 17.

[13] U. Ali, R. Liaqat, A. Algahtani, S. Mujtaba, V. Tirth, A.M. Alsuhaibani, M.S. Refat, A. Ali, M. Aslam, A. Zaman, Analysis and characterization of opto-electronic properties of iron oxide (Fe2O3) with transition metals (Co, Ni) for the use in the photodetector application, J. Mater. Res. Technol. 25 (2023) 6150–6166.

[14] A. Alsulmi, N.N. Mohammed, M.M. Hassan, M.A. Eltawil, A.E. Amin, M. Fahmy, M.A. Ahmed, Rational engineering of S-scheme CeO2/g-C3N4 heterojunctions for effective photocatalytic destruction of rhodamine B dye under natural solar radiations, Colloids Surf., A 689 (2024) 133683.

[15] W. Xue, H. Sun, X. Hu, X. Bai, J. Fan, E. Liu, UV-VIS-NIR-induced extraordinary H2 evolution over W18O49/Cd0.5Zn0.5S: surface plasmon effect coupled with S-scheme charge transfer, Chin. J. Catal. 43 (2022) 234–245.

[16] Abanoob M. Basely, Mohamed H. Shaker, Fatma M. Helmy, M.F. Abdel-Messih, M.A. Ahmed, Construction of Bi2S3/g-C3N4 step S-scheme heterojunctions for photothermal decomposition of rhodamine B dye under natural sunlight radiation, Inorg. Chem. Commun. 148 (2023) 110300.

[17] Alsalme Ali, A.H. Galal, Essam Foad El-Sherbeny, Ayman Soltan, M.F. Abdel-Messih, M.A. Ahmed, Fabrication of S-scheme TiO2/g-C3N4 nanocomposites for generation hydrogen gas and removal of fluorescein dye, Diamond Related Matters 122 (2022) 108819.

[18] Alsulmi Ali, Mohamed H. Shaker, Abanoob M. Basely, M.F. Abdel-Messih, Ayman Sultan, M.A. Ahmed, Engineering S-scheme Ag2CO3/g-C3N4 heterojunctions sonochemically to eradicate Rhodamine B dye under solar irradiation, RSC Adv. 13 (2023) 12229.

[19] H.S.M. Abd-Rabboh, A.H. Galal, A.M. Basely, F.M. Helmy, M.A. Ahmed, Boosting hydrogen gas production and mitigation of fluorescein dye on the surface of S-scheme g-C3N4/SnO2 heterojunction, Desalination Water Treat. 268 (2022) 113–125.

[20] Nabil Al-Zaqri, Alsalme Ali, M.A. Ahmed, A.H. Galal, Construction of novel direct Z-scheme AgIO4-g-C3N4 heterojunction for photocatalytic hydrogen production and photodegradation of fluorescein dye, Diamond related matters 109 (2020) 108071.

[21] M. Assis, C.C. de Foggi, V. Teodoro, J.P. de Campos da Costa, C.E. Silva, T. Robeldo, P.F. Caperucci, C.E. Vergani, R.C. Borra, I. Sorribes, A.E.F. Gouveia, M. A. San-Miguel, J. Andres, Elson Longo, Surface-dependent photocatalytic and biological activities of Ag2CrO4: integration of experiment and simulation, Appl. Surf. Sci. 545 (2021) 148964.

[22] G.S. Silva, L. Gracia, M.T. Fabbro, L.P. Serejo dos Santos, H. Beltran-Mir, ′E. Cordoncillo, E. Longo, J. Andres, Theoretical and experimental insight on Ag2CrO4 microcrystals: synthesis, characterization, and photoluminescence properties, Inorg. Chem. 55 (2016) 8961–8970.

[23] M.T. Fabbro, L. Gracia, G.S. Silva, L.P.S. Santos, J. Andres, E. Cordoncillo, E. Longo, Understanding the formation and growth of Ag nanoparticles on silver chromate induced by electron irradiation in electron microscope: a combined experimental and theoretical study, J. Solid State Chem. 239 (2016) 220–227.

[24] J. Zhang, W. Yu, J. Liu, B. Liu, Illustration of high-active Ag2CrO4 photocatalyst from the first-principle calculation of electronic structures and carrier effective mass, Appl. Surf. Sci. 358 (2015) 457–462.

[25] M. Assis, C.C. de Foggi, V. Teodoro, J.P.D. da Costa, C.D. Silva, T. Robeldo, P.F. Caperucci, C.E. Vergani, R.C.B.I. Sorribes, A.F. Gouveia, M.A. San-Miguel, J. Andres, E. Longo, Surface-dependent photocatalytic and biological activities of Ag2CrO4: integration of experiment and simulation, Appl. Surf. Sci. 545 (2021) 148964.

[26] F. Yu, J. Cui, Y. Zhou, Y. Li, Z. Liu, Ling He a, J. Zhang, X. Tang Y. Liu, Structural and Optical Properties of Ultra-thin g-C3N4 nanotubes based g-C3N4/Ag/ Ag2CrO4 ternary composite photocatalyst with Z-scheme carrier transfer mechanism, Opt. Mater. 121 (2021) 111608.

[27] X. Ren, X. Zhang, R. Guo, X. Li, Y. Peng, X. Zhao, X. Pu, Hollow mesoporous g-C3N4/Ag2CrO4 photocatalysis with direct Z-scheme: excellent degradation performance for antibiotics and dyes, Sep. Purif. Technol. 270 (2021) 118797.

[28] N. Rajalakshmi, D. Barathi, S. Meyvel, P. Sathya, S-scheme Ag2CrO4/g-C3N4 photocatalyst for effective degradation of organic pollutants under visible light, Inorg. Chem. Commun. 132 (2021) 108849.

[29] Y. Che, B. Lu, QiQi, H. Chang, J. Zhai, K. Wang, Z. Liu, Bio-inspired Z-scheme g-C3N4/Ag2CrO4 for efficient visible light photocatalytic hydrogen generation, Scientific report 8 (2018) 16504.

[30] Anise Akhundi, Aziz Habibi-Yangjeh, Codeposition of AgI and Ag2CrO4 on g-C3N4/Fe3O4 nanocomposite: novel magnetically separable visible-light-driven photocatalysts with enhanced activity, Adv. Powder Technol. 27 (2016) 2496–2506.

[31] Aziz Habibi-Yangjeh, Anise Akhundi, Novel ternary g-C3N4/Fe3O4/Ag2CrO4 nanocomposites: magnetically separable and visible-light-driven photocatalysts for degradation of water pollutants, J. Mol. Catal. 415 (2016) 122–130.

[32] Y. Shang, X. Chen, W. Liu, P. Tan, H. Chen, L. Wu, C. Ma, X. Xiong, J. Pan, Photocorrosion inhibition and high-efficiency photoactivity of porous g-C3N4/ Ag2CrO4 composites by simple microemulsion-assisted co-precipitation method, Appl. Catal. 204 (2017) 78–88.

[33] Y. Liu, H. Yu, M. Cai, J. Sun, Microwave hydrothermal synthesis of Ag2CrO4 photocatalyst for fast degradation of PCP-Na under visible light irradiation, Catal. Commun. 26 (2012) 63–67.

[34] Y. Shang, H. Fan, X. Yang, W. Dong, W. Wang, Synergism between chemisorption and unique electron transfer pathway in S-scheme AgI/g-C3N4 heterojunction for improving the photocatalytic H2 evolution, J. Colloid Interface Sci. 631 (2023) 269–280.

[35] S. Wageh, A.A. Al-Ghamdi, R.J.X. Li, Peng Zhang, A new heterojunction in photocatalysis: S-scheme heterojunction, Chin. J. Catal. 42 (2021) 667–669.

[36] S. Jiang, J. Cao, M. Guo, D. Cao, X. Jia, H. Lin, Shifu Chen, Novel S-scheme WO_3/RP composite with outstanding overall water splitting activity for H_2 and O_2 evolution under visible light, Appl. Surf. Sci. 558 (2021) 149882.

[37] X. Zhang, Y. Zhang, X. Jia, N. Zhang, R. Xia, X. Zhang, Z. Wang, M. Yu, In situ fabrication of a novel S-scheme heterojunction photocatalyts Bi_2O_3/P-C_3N_4 to enhance levofloxacin removal from water, Sep. Purif. Technol. 268 (2021) 118691.

[38] Ke Zhang D. Li, Q. Tian, H. Cao, F. Orudzhev, I.A. Zvereva, J. Xu, C. Wang, Recyclable 0D/2D $ZnFe_2O_4$/$Bi_5FeTi_3O_{15}$ S-scheme heterojunction with bismuth decoration for enhanced visible-light-driven tetracycline photodegradation, Ceram. Int. 47 (2021) 17109–17119.

[39] S. Wu, X. Yu, J. Zhang, Y. Zhang, Y. Zhu, M. Zhu, Construction of $BiOCl$/$CuBi_2O_4$ S-scheme heterojunction with oxygen vacancy for enhanced photocatalytic diclofenac degradation and nitric oxide removal, Chem. Eng. J. 411 (2021) 128555.

[40] V.V. Pham, D.Q. Mai, D.P. Bui, T.V. Man, B. Zhu, L. Zhang, J. Sangkaworn, J. Tantirungrotechai, V. Reutrakul, T.M. Cao, Emerging 2D/0D g-C_3N_4/SnO_2 S-scheme photocatalyst: new generation architectural structure of heterojunctions toward visible-light-driven NO degradation, Environ. Pollut. 286 (2021) 117510.

[41] H. Huang, Y.X. Li, H.L. Wang, Wen-Feng Jiang, in situ fabrication of ultrathin-g-C_3N_4/AgI heterojunctions with improved catalytic performance for photodegrading rhodamine B solution, Appl. Surf. Sci. 538 (2021) 148132.